ELSEVIER

Contents lists available at ScienceDirect

International Journal of Rock Mechanics and Mining Sciences

journal homepage: http://www.elsevier.com/locate/ijrmms





Three-dimensional stability assessment of slopes in intact rock governed by the Hoek-Brown failure criterion

Dowon Park ^a, Radoslaw L. Michalowski ^{b,*}

- a Department of Civil Engineering, University of Seoul, 163 Seoulsiripdae-ro Dongdaemun-gu, Seoul, 02504, South Korea
- b Department of Civil and Environmental Engineering, University of Michigan, 2028 G.G. Brown Bldg 2350 Hayward, Ann Arbor, MI, 48109, USA

ARTICLE INFO

Keywords: Rock slope stability 3D limit analysis Hoek-Brown strength envelope Factor of safety Stability number

ABSTRACT

Three-dimensional failure analyses of slopes are rather elaborate, and for rock slopes, where the rock strength is defined by nonlinear failure envelopes, they are particularly intricate. This is why many earlier approaches used a linear approximation of the strength envelope prior to carrying out the stability analysis. This approximation is avoided in this paper, thanks to using the parametric form of the Hoek-Brown failure criterion. The kinematic approach of limit analysis is used as the method of study. An argument is brought forward that even though rocks tend to fracture at low confining stresses, the ductility of deformation prior to a brittle drop in stress during failure may be sufficient for limit analysis theorems to be applicable. Two measures of rock slope stability are evaluated: the stability number and the factor of safety. Numerical results are presented in the form of charts and tables. Because the limit analysis used allows one to evaluate the rigorous bounds on true solutions, it was possible to demonstrate that the method employed in the paper yields more accurate results than the approaches used formerly in the subject literature. A new and efficient mechanism of failure was devised for very narrow rock slopes.

1. Introduction

While two-dimensional (2D) stability analyses of slopes have been extensively investigated for both soils and rocks, considerations of three-dimensional (3D) failures have been less common, particularly for geomaterials with strength governed by non-linear envelopes. When the size of a slope failure mechanism is limited by physical constraints, such as nearby structures, the use of 2D (or plane-strain) analyses will underestimate the stability of a slope, so a 3D analysis is preferred. Admissible failure mechanisms are explored in this paper for intact rocks with strength governed by the Hoek-Brown failure criterion. ^{1,2} A 3D mechanism proposed earlier for soil slopes by Michalowski and Drescher³ has been adapted to accommodate the non-linearity of the pressure dependency of rock strength. Special attention is paid to narrow rock slopes where a new type of *ridge failure surface mechanism* is constructed.

Typical limit analyses of slopes in geomaterials with nonlinear dependency of strength on pressure involve linearization of the failure criterion in the first invariant of the stress tensor. Effectively, the nonlinear failure envelope in this approach is replaced by a straight line, and the stability problem is solved for a linear, or an *equivalent Mohr-*

Coulomb criterion, which greatly simplifies calculations. The early examples of such an approach can be found in Drescher and Christopoulos⁴ and others. 5,6 This is the most often encountered approach in considerations of both 2D and 3D stability of rock slopes. The linear approximation was employed in many recent 3D slope stability studies.^{7–11} Essentially, this approach ignores the nonlinearity of the strength envelope; consequently, it disregards a group of admissible failure mechanisms that can only be constructed for nonlinear failure criteria. This shortcoming was overcome in a recent 2D stability analysis by Michalowski and Park, $^{12}\,\mathrm{for}\,\mathrm{slopes}$ with strength governed by the Hoek-Brown failure criterion. Efficient application of limit analysis requires an explicit form of the rock shear strength τ as a function of normal stress σ'_n on failure surfaces. Because the original form of the Hoek-Brown criterion is a function of principal stresses, the criterion is often approximated in the analysis with a best-fit function $\tau = f(\sigma'_n)$. This step was avoided in this study by using the parametric form of the original criterion, whereas the common linearization procedure was overcome by allowing rock failure at varying rupture angles in a single collapse mechanism. This analysis is now extended to 3D stability of rock slopes, which introduces additional challenges, because of the complexity of the

E-mail addresses: dowon@uos.ac.kr (D. Park), rlmich@umich.edu (R.L. Michalowski).

^{*} Corresponding author.

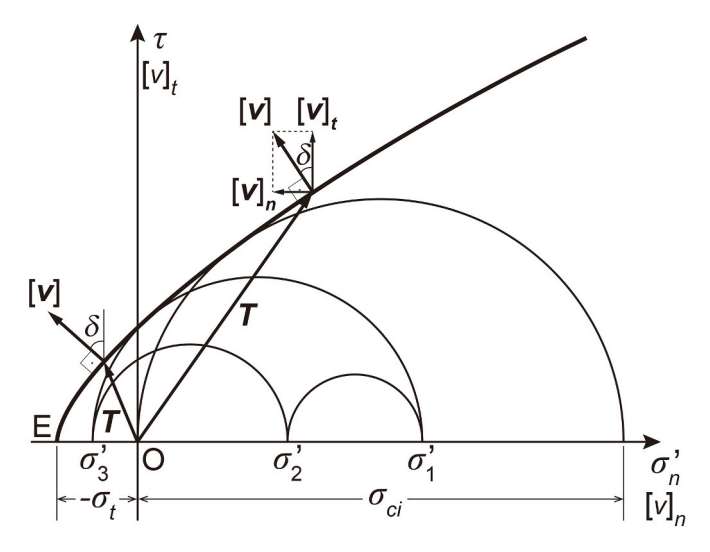


Fig. 1. Hoek-Brown strength envelope.

mechanism.

The limit analysis approach to rocks is briefly discussed next, followed by a short description of the Hoek-Brown failure criterion. The mechanisms of rock slope failure are presented in subsequent sections, and the quantitative outcome of the analysis is presented in charts and tables with stability numbers and factors of safety.

2. Application of limit analysis in rocks, and the Hoek-Brown strength criterion

2.1. Limit analysis in rock applications

Limit Analysis is a method used extensively in structural engineering, geotechnical engineering, and plastic forming of metals. The fundamental premise of the method is perfectly plastic behavior of the material with the convex limit stress criterion and the normality flow rule. However, the ductility of rock behavior can be questioned as rocks tend to fracture at low confining stresses. This issue was discussed by Chen, ho concluded that if the rock strain is small prior to an "appreciable" (brittle) fall off of the stress, then the deformability "may be sufficient to permit the consideration of limit theorems ..." Consequently, applications of limit analysis in rocks can be found throughout the literature (e. g., Chen and Drucker, 14 Michalowski, 15 Fraldi et al. 16).

2.2. Hoek-Brown failure criterion

The Hoek-Brown failure criterion dates back to 1980^{17} , with its generalized form given in the following 1,2

$$\sigma_1' = \sigma_3' + \sigma_{ci} \left(m_b \frac{\sigma_3'}{\sigma_{ci}} + s \right)^a \tag{1}$$

where σ_1' and σ_3' are the major and minor effective principal stresses, respectively, σ_{ci} is the compressive strength of the intact rock, and the remaining strength parameters are defined as

$$m_b = m_i e^{\left(\frac{GSJ - 100}{2S - 14D}\right)} \tag{2}$$

$$a = \frac{1}{2} + \frac{1}{6} \left(e^{-\frac{GSI}{15}} - e^{-\frac{20}{3}} \right) \tag{3}$$

and

$$s = e^{\left(\frac{GS - 100}{9 - 3D}\right)} \tag{4}$$

where GSI, m_i and D are the Geological Strength Index, rock type-dependent parameter, and the disturbance factor, respectively. The failure envelope in Eq. (1) is illustrated in Fig. 1. The uniaxial compressive strength σ_{ci} is an explicit part of the criterion in Eq. (1), whereas the isotropic tensile strength σ_t (corresponding to point E in Fig. 1), can be easily found from Eq. (1) after substituting $\sigma_1' = \sigma_2' = \sigma_2' = -\sigma_t$

$$\sigma_t = \sigma_{ci} \frac{s}{m_t} \tag{5}$$

The Limit Analysis approach used in the paper requires that the deformation of the rock at failure is governed by the normality flow rule, and vectors [v], normal to the strength envelope in Fig. 1, are the velocity discontinuity vectors inclined at rupture angle δ to the failure surfaces (kinematic discontinuities).

Direct calculations of the rate of work dissipation on failure surfaces call for an explicit form of the shear strength as function of the normal stress $\tau=f(\sigma_n')$. Such a form cannot easily be found directly from Eq. (1), and in many previous analyses the nonlinear criterion was either replaced with a linear approximation or with a 'best fit' function in a desirable range of stresses. To avoid such approximations, a parametric form of the strength criterion will be used. Following earlier developments, 18,19 both the normal and the shear stresses are expressed as functions of rupture angle δ

$$\sigma_n = \sigma_{ci} \left\{ \left(\frac{1}{m_b} + \frac{\sin \delta}{m_b a} \right) \left[\frac{m_b a (1 - \sin \delta)}{2 \sin \delta} \right]^{\frac{1}{1 - a}} - \frac{s}{m_b} \right\}$$
 (6)

$$\tau = \sigma_{ci} \left\{ \frac{\cos \delta}{2} \left[\frac{m_b a (1 - \sin \delta)}{2 \sin \delta} \right]^{\frac{a}{1 - a}} \right\}$$
 (7)

Rupture angle δ is illustrated in Fig. 1.

2.3. Measures of rock slope stability

Two measures of rock slope stability are considered in this paper: $stability number \ N$ and $factor \ of \ safety \ F$. The former is defined as a dimensionless combination of the rock properties and the slope height, at which the slope collapse becomes imminent, and it is adopted after Collins et al.⁵ This dimensionless group is defined as a critical combination

$$N = \left(\frac{\sigma_{ci}}{\gamma H}\right)_{crit} \tag{8}$$

where σ_{ci} , γ and H and are the uniaxial compressive strength of intact rock, its unit weight, and the slope height, respectively. This measure was chosen so that the computational outcomes in this paper can be compared with data available in the literature. Stability number N is a reciprocal of the *stability factor*¹³; both carry identical information, but, historically, the stability number has been used more often, because of the ease of presenting graphical data with a higher resolution. ²⁰ This is despite the fact that of the two, the stability number is less intuitive, as it increases with an increase in the angle of slope inclination. Safe slopes have the dimensionless group $\sigma_{ci}/\gamma H$ higher than the stability number, whereas the opposite is true for the stability factor. The concept was first used in defining stability of soil slopes by Taylor, ²⁰ and it was used for rock slopes with the strength defined by the Hoek-Brown criterion by Collins et al.⁵

The second stability measure, factor of safety F, is defined as the ratio of the shear strength of intact rock τ to the demand on the shear strength τ_d needed for stability

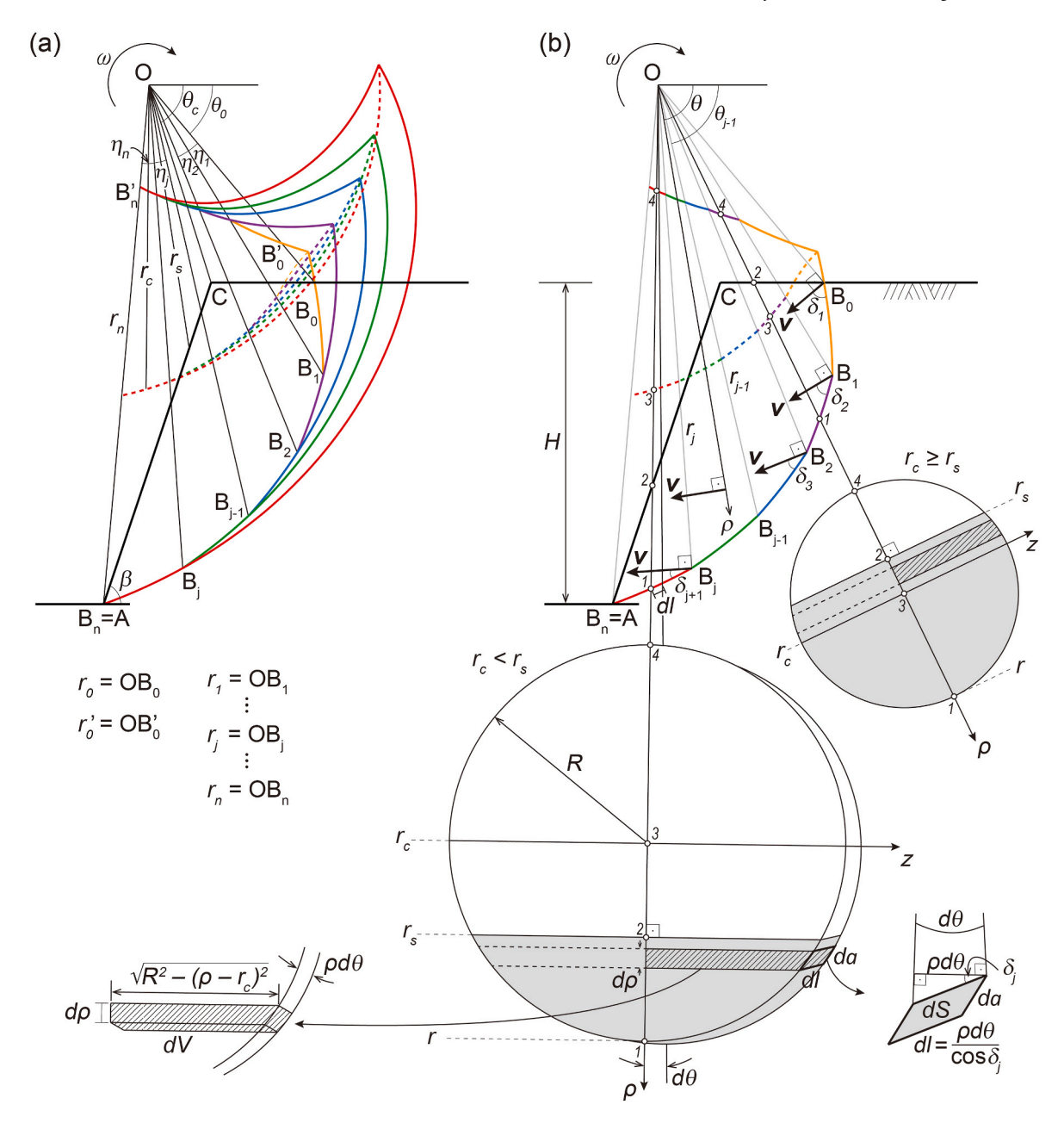


Fig. 2. Three-dimensional rotational multi-cone failure mechanism in intact rock: (a) central cross-section showing contours of multiple cones, and (b) contour of the rotating block and radial plane cross-sections of the multi-cone failure surface.

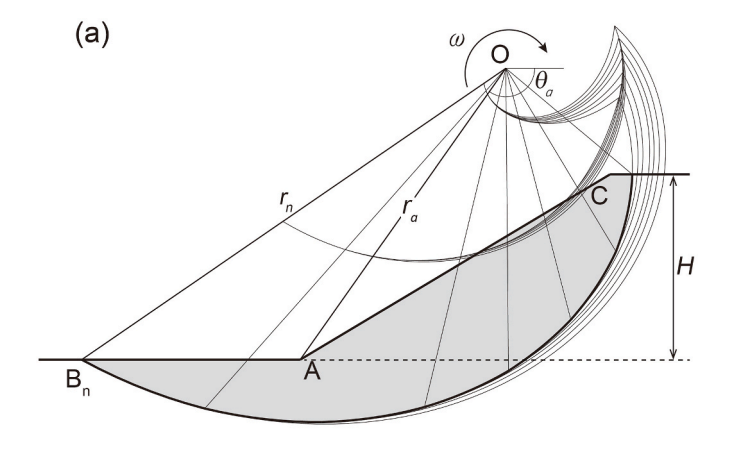
$$F = \frac{\tau}{\tau_d} \tag{9}$$

Factor of safety F is a common measure used in geotechnical engineering, but its use is somewhat intricate in stability analyses with strength envelopes that exhibit non-linear pressure dependency, such as the Hoek-Brown criterion. This is why attempts were made in the past to define the factor of safety for rock slopes using the uniaxial compressive strength, 21 rather than the shear strength. While such an approach leads to a simple explicit solution for the slope safety factor, it is not consistent with the definition in Eq. (9), and it significantly overestimates factors of safety produced by Eq. (9). This matter was discussed at a greater length in an earlier paper. 12

3. Three-dimensional multi-cone failure mechanism

3.1. Mechanism geometry

Collapse of slopes in rocks often follows the joints, which form weak planes in the rock mass. However, slopes in intact rock with fairly isotropic strength are susceptible to rotational failures. Failure surfaces in such collapse mechanisms are likely to be curvilinear and their specific geometry in the analysis needs to be consistent with the restrictions imposed by the normality of deformation enforced in limit analysis. A rigid rotational collapse mechanism is considered, and the concept of a curvilinear cone in Michalowski²² and Michalowski and Drescher³ is employed here. The curvilinear cone mechanism was adopted earlier in analyses of slopes in geomaterials governed by the Mohr-Coulomb strength envelope modified with a nonlinear tension cutoff, ^{23,24} but the cut-off criterion is not universally accepted in rock engineering, and a new multi-cone mechanism is developed here to specifically



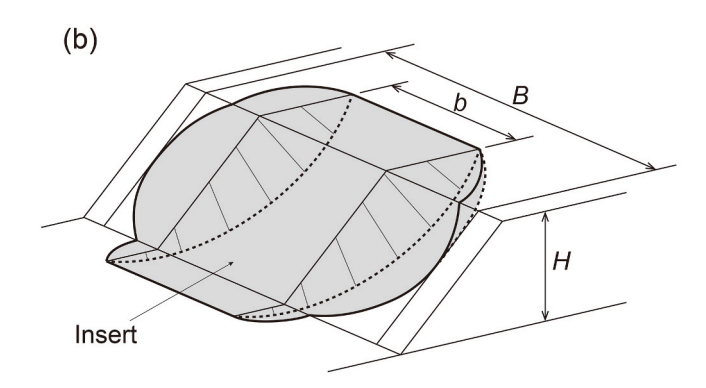


Fig. 3. Below toe failure mechanism: (a) central cross-section, and (b) insert between two halves of the multi-cone failure mechanism.

accommodate the Hoek-Brown strength criterion in the analysis. An important extension of the method is made to accommodate varying rupture angle δ allowed by the nonlinearity of the Hoek-Brown failure envelope (Fig. 1). Rather than using one curvilinear cone surface with a single value of rupture angle δ (or internal friction angle in case of soils), a series of cones is used here, each with a different rupture angle.

A schematic of the multi-cone mechanism is illustrated in Fig. 2. The slope is homogeneous, with inclination angle β . At failure, the rock mass with cross-section $CB_0B_1B_jB_nC$ rotates about an axis passing through point O. The rotating rock block consists of n segments, each segment limited by the contour of the slope and the failure surface, and the segments are separated from one another by radial planes. For example, segment j=2 is separated from neighboring segments by planes OB_1 and OB_2 , and is separated from the stationary rock by the failure surface cross-section B_1B_2 . Rupture angle δ is constant within an individual segment, but it varies from segment to segment owed to nonlinearity of the failure envelope, Fig. 1. All segments form one rotating rock block, with no sliding between the segments, and failure surface $B_0B_1B_jB_n$ consists of log-spiral sections, each with different rupture angle δ .

The entire failure surface is constructed of n segments, each being a part of a different curvilinear cone, as illustrated in Fig. 2(a). The lower contour of the cone that comprises the jth segment is defined by the following log-spiral

$$r(\theta) = r_{j-1}e^{\left(\theta - \theta_{j-1}\right)\tan \delta_j} , \quad \theta_{j-1} \le \theta \le \theta_j$$
 (10)

where r_{j-1} is the radius of the j-1st cone at angular coordinate θ_{j-1} , Fig. 2 (b), and is determined from the following expression

$$r_{j-1} = r_0 e^{\sum_{k=1}^{j-1} (\theta_k - \theta_{k-1}) \tan \delta_k}$$
 (11)

The upper contour of the jth log-spiral cone is defined by

$$r'(\theta) = r'_{j-1} e^{-\left(\theta - \theta_{j-1}\right) \tan \delta_j} , \quad \theta_{j-1} \le \theta \le \theta_j$$
(12)

where

$$r_{j-1}' = r_0' e^{-\sum_{k=1}^{j-1} (\theta_k - \theta_{k-1}) \tan \delta_k}$$
 (13)

and ratio r_0^\prime/r_0 is one of the independent variables in constructing the mechanism. A radial cross-section of every cone has a circular cross-section of radius R

$$R(\theta) = \frac{r(\theta) - r'(\theta)}{2} \tag{14}$$

and the center of the circular cross-section is located at distance r_c from point O

$$r_c(\theta) = \frac{r(\theta) + r'(\theta)}{2} \tag{15}$$

A cross-section of a below-toe multi-cone failure mechanism is illustrated in Fig. 3(a). To assure that the mechanism will tend to a 2D mechanism if no limitation is imposed on its width, an insert of width b is placed between two symmetric halves of the multi-cone mechanism as shown in Fig. 3(b). Given limitation B on the total width of the entire mechanism, width b of the insert can be determined as the smaller of the following two values

$$b = B - 2 \cdot \max(R), r_c \ge r_s$$

$$b = B - 2 \cdot \max\left[\sqrt{R^2 - (r_s - r_c)^2}\right], r_c < r$$
(16)

where R and r_c are given in Eqs. (14) and (15), and r_s is the slope contour radius in Eq. (A3). For below-toe failure mechanisms, point B_n with coordinates r_n , θ_n is not located at the toe, and polar coordinate θ_a defines the location of toe A, with the radial coordinate

$$r_a = r_n \frac{\sin \theta_n}{\sin \theta_n} \tag{17}$$

3.2. Rates of work dissipation and gravity work

The kinematic approach of limit analysis is based on the theorem stating that the rate of plastic work (dissipated) in an incipient failure process is not less than the rate of work of external forces in any kinematically admissible mechanism. For slopes failing along failure surface *L* and loaded with gravity forces, the theorem entails only two terms

$$\int_{L} T_{i}[v]_{i} dL \ge \int_{V} X_{i} v_{i} dV \tag{18}$$

where the term on the left side represents the rate of work dissipation and the term on the right-hand side is the work rate of gravity forces X_i acting in the mechanism with volume V. Stress vector T_i on failure surfaces and the velocity discontinuity vector $[v]_i$ are illustrated in Fig. 1. Rigorous bounds to specific stability measures are calculated from the balance equation, which assumes that the two terms in theorem (18), dissipation D and gravity work rate W_v are equal to one another

$$D = W_{y} \tag{19}$$

Rate of work dissipation d per unit area of the failure surface is found as

$$d = [v](\tau \cos \delta - \sigma_n \sin \delta) \tag{20}$$

where [v] is the magnitude of the velocity discontinuity vector [v] on the rupture surface; τ and σ_n are the components of the stress vector T on the failure surface (Fig. 1). Total rate of work dissipation D is calculated by integrating the rate per unit area in Eq. (20) over entire rupture

surface S

$$D = \int_{c} [v](\tau \cos \delta - \sigma_n \sin \delta) dS$$
 (21)

Infinitesimal surface element dS is illustrated on the bottom right in Fig. 2(b)

$$dS = dl da = \frac{\rho}{\cos \delta_j} \frac{R}{\sqrt{R^2 - (\rho - r_c)^2}} d\rho d\theta$$
 (22)

With $[v] = \omega \rho$ (ω - angular velocity about axis through point O), the rate of work dissipation over the entire 3D rupture surface is determined by

$$D = 2\omega \sum_{j=1}^{n} \left(\tau_{j} - \sigma_{nj} \tan \delta_{j}\right) \int_{\theta_{j-1}}^{\theta_{j}} \int_{r_{s}}^{r} \rho^{2} \frac{R}{\sqrt{R^{2} - (\rho - r_{c})^{2}}} d\rho d\theta$$
 (23)

where ρ is the radial polar coordinate (Fig. 2(b)), and r_s is the radial coordinate of the slope contour expressed in Eq. (A3). When a plane insert of width b is included in the mechanism, as in Fig. 3(b), the work dissipation takes the form

$$D = \omega \sum_{j=1}^{n} \left(\tau_{j} - \sigma_{nj} \tanh \delta_{j} \right) \int_{\theta_{i-1}}^{\theta_{j}} \left[\int_{r_{c}}^{r} \rho^{2} \frac{2R}{\sqrt{R^{2} - (\rho - r_{c})^{2}}} d\rho + b r^{2} \right] d\theta$$
 (24)

where r is expressed in Eq. (10).

Rate of work of gravity forces W_{γ} in the mechanism can be expressed as

$$W_{\gamma} = \int_{V} \gamma v \cos \theta dV \tag{25}$$

where γ is the unit weight of rock, and dV is the infinitesimal volume shown in the bottom left of Fig. 2(b)

$$dV = \sqrt{R^2 - (\rho - r_c)^2} \rho \, d\rho d\theta \tag{26}$$

Summing up the work rate in all n segments of the rotating block, the total gravity work rate becomes

$$W_{\gamma} = 2\omega\gamma \sum_{j=1}^{n} \int_{\theta_{j-1}}^{\theta_{j}} \int_{r_{s}}^{r} \rho^{2} \sqrt{R^{2} - (\rho - r_{c})^{2}} \cos\theta d\rho d\theta$$
 (27)

and, with the inclusion of the insert, it takes the form

$$W_{\gamma} = \omega \gamma \sum_{j=1}^{n} \int_{\theta_{j-1}}^{\theta_{j}} \int_{r_{s}}^{r} \rho^{2} \left[2\sqrt{R^{2} - (\rho - r_{c})^{2}} + b \right] \cos \theta d\rho d\theta$$
 (28)

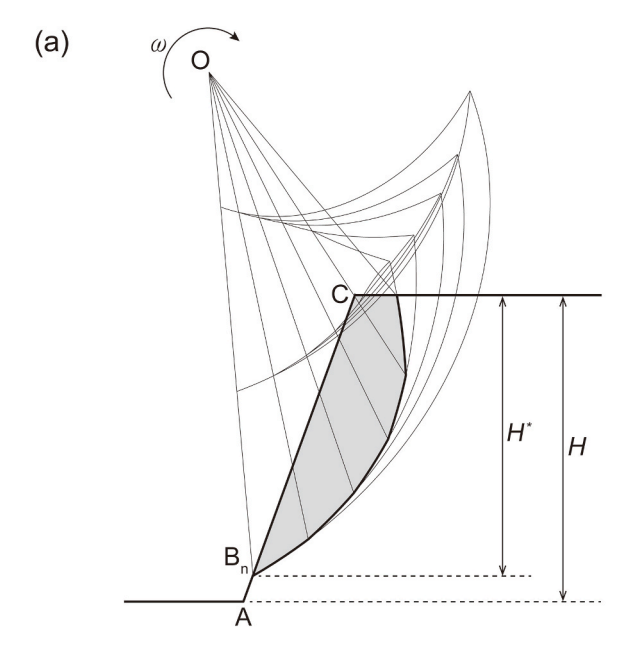
where *b* stands for the width of the insert.

Negative width b of the insert following from Eq. (16) indicates that the mechanism constructed cannot be contained within width B. In such a case, a face failure mechanism or a ridge failure surface mechanism is likely, as described in the following section.

4. Multi-cone face failure and ridge mechanisms

4.1. Face failure mechanism

The size of a 3D slope failure mechanism is limited by constraint B, as illustrated in Fig. 3(b). Such a constraint may be owed, for example, to an outcrop of a stronger rock. For a very stringent constraint B/H, a rotational mechanism that reaches the toe of the slope may violate this width restriction. There is a lower limit on ratio B/H for a given slope



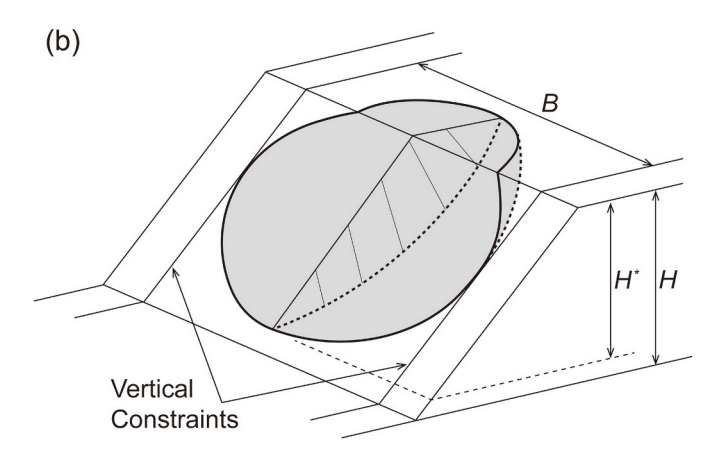


Fig. 4. Face failure multi-cone mechanism: (a) central cross-section, and (b) view of the failure surface.

inclination, for which an admissible toe rotational collapse mechanism can be constructed. If this limit is $(B/H)^*$, then for $B/H < (B/H)^*$ one can construct an admissible mechanism, but this mechanism will not reach the toe, as illustrated in Fig. 4(a). If the stability number (Eq. (8)) for the limit case $(B/H)^*$ is denoted as N^* , then stability number N for cases where $B/H < (B/H)^*$ can be calculated as

$$N = N^* \frac{\frac{B}{H}}{\left(\frac{B}{H}\right)} \tag{29}$$

The mechanisms associated with $B/H < (B/H)^*$ are then face failure mechanisms as illustrated in Fig. 4. Because $(B/H)^*$ and N^* are both constant for a given slope inclination, the stability number for narrow slopes becomes a linear function of ratio B/H, as in Eq. (29). This was discussed earlier in Park and Michalowski.²⁵

4.2. Multi-cone ridge surface failure mechanism

The second option in constructing a failure mechanism in a narrow space is considered below. This is also a face failure mechanism, but it is constructed by removing a central portion of width b^* from the rotating rock block shown in Fig. 2, in order to make the mechanism fit into the

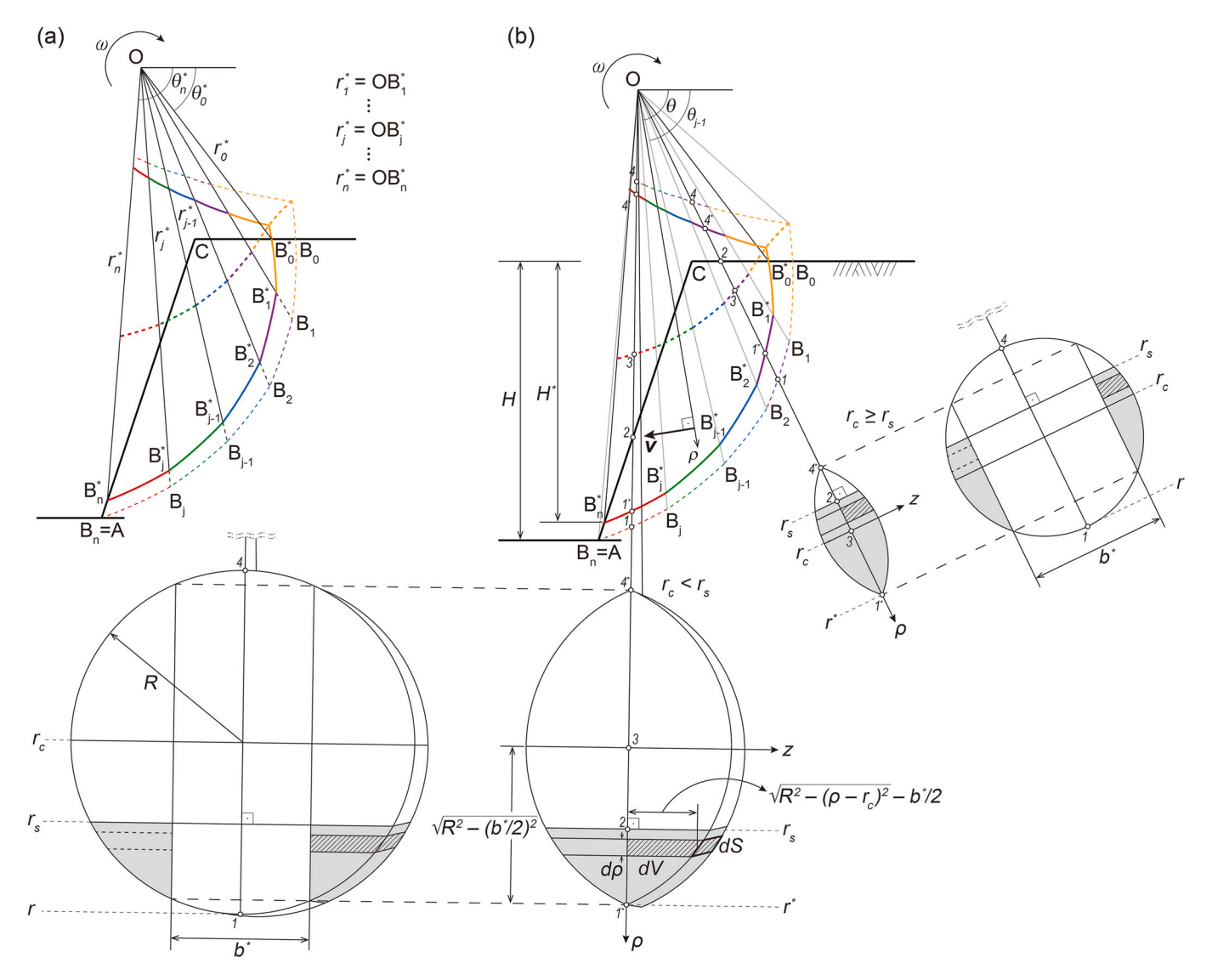


Fig. 5. Multi-cone ridge failure surface mechanism: (a) central cross-section, and (b) radial cross-sections of the failure surface.

narrow space. In other words, if the mechanism width is too large to fit into a constrained failure space, an "excess" width is removed from the middle portion of the mechanism (as opposed to adding an insert for wider slopes). The concept of such a mechanism is illustrated in Fig. 5. Excess width b^* is the larger of the two expressions

$$b^* = 2 \cdot \max(R) - B , \qquad r_c \ge r_s$$

$$b^* = 2 \max \left[\sqrt{R^2 - (r_s - r_c)^2} \right] - B , \quad r_c < r_s$$
(30)

where R, r_c and r_s are all functions of θ , and are expressed in Eqs. (14), (15) and (A3), respectively. The trace of original failure surface $B_0B_1B_2B_jB_n$ on the symmetry plane consists of log-spiral sections, as the one in Fig. 5 (or Fig. 2) does. Once the mid-portion of width b^* is removed from the mechanism, the remaining symmetric halves are moved together to form a distinct ridge, as illustrated on radial cross-sections in Fig. 5(b). Originally smooth circular cross-sections of the curvilinear cones become oval, with clear discontinuities in the derivative. However, the newly formed ridge $B_0^*B_1^*B_2^*B_3^*$ is not formed of sections of log-spirals, and its radius r^* is given in the following expression

$$r^*(\theta) = r_c(\theta) + \sqrt{R^2(\theta) - \left(\frac{b^*}{2}\right)^2}, \quad \theta_0^* \le \theta < \theta_n^*$$
 (31)

where θ_0^* and θ_n^* are the angular coordinates of point B_0^* on the top surface and point B_n^* on the inclined surface of the slope just above the toe. Both θ_0^* and θ_n^* can be found from an implicit equation (iteratively solved) that makes use of the condition that both B_0^* and B_n^* are located on the slope surface defined by radius r_s , Eq. (A3)

$$r_c(\theta^*) + \sqrt{R^2(\theta^*) - \left(\frac{b^*}{2}\right)^2} = r_s(\theta^*)$$
 (32)

4.3. Rates of work in the ridge mechanism

The rate of work dissipation over a 3D rupture surface is determined by

$$D = 2\omega \sum_{j=1}^{n} (\tau_{j} - \sigma_{nj} \tan \delta_{j}) \int_{\theta_{j-1}}^{\theta_{j}} \int_{r_{s}}^{r^{*}} \rho^{2} \frac{R}{\sqrt{R^{2} - (\rho - r_{c})^{2}}} d\rho d\theta$$
 (33)

The difference from Eq. (23) is in the limits of integration: the upper

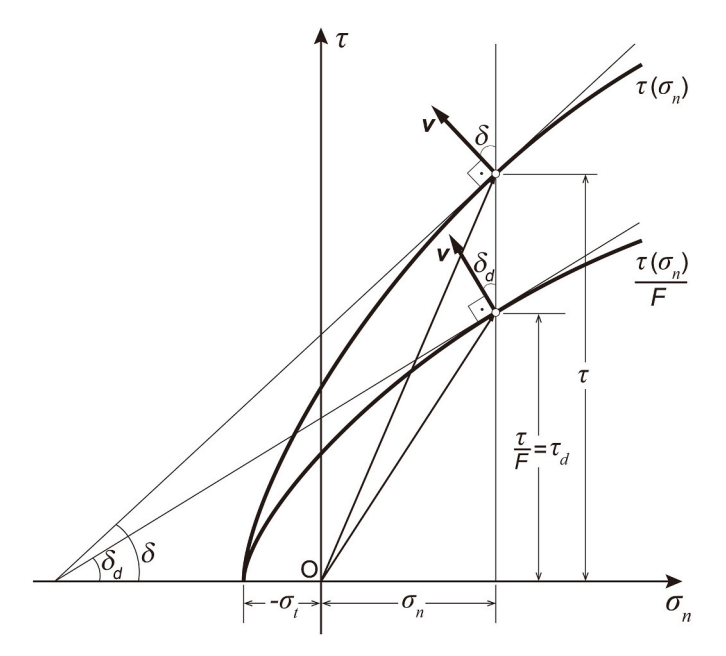


Fig. 6. Hoek-Brown strength envelope and the envelope reduced by factor of safety F.

limit on the radius now is r^* , the lower limit on the angular coordinate in the first sector is θ_n^* , and the upper limit in the last sector is θ_n^* , both evaluated from Eq. (32). With the exclusion of the slice of width b^* from the mechanism, Fig. 5, the infinitesimal volume element is modified

$$dV = \left(\sqrt{R^2 - (\rho - r_c)^2} - \frac{b^*}{2}\right)\rho \,d\rho d\theta \tag{34}$$

and the work rate of rock weight during infinitesimal failure becomes

$$W_{\gamma} = \omega \gamma \sum_{j=1}^{n} \int_{\theta_{j-1}}^{\theta_{j}} \int_{r_{s}}^{r^{*}} \rho^{2} \left[2\sqrt{R^{2} - (\rho - r_{c})^{2}} - b^{*} \right] cos\theta d\rho d\theta$$
 (35)

5. Stability measures

5.1. Stability number

Substituting the work rate expressions in Eqs. (24) and (28) into Eq. (19), the following expression is derived for dimensionless group $\sigma_{ci}/\gamma H$ for a failure mechanism with an insert

$$\frac{\sigma_{ci}}{\gamma H} = \frac{\sum\limits_{j=1}^{n} \int\limits_{\theta_{j-1}}^{\theta_{j}} cos\theta \int\limits_{r_{s}}^{r} \rho^{2} \left[2\sqrt{R^{2} - (\rho - r_{c})^{2}} + b \right] d\rho d\theta}{\frac{H}{\sigma_{ci}} \sum\limits_{j=1}^{n} \left(\tau_{j} - \sigma_{nj} \ tan\delta_{j} \right) \int\limits_{\theta_{j-1}}^{\theta_{j}} \left[\int\limits_{r_{s}}^{r} \rho^{2} \frac{2R}{\sqrt{R^{2} - (\rho - r_{c})^{2}}} d\rho + b \ r^{2} \right] d\theta}$$
(36)

The maximized value of the expression in Eq. (36) is the stability number as defined in Eq. (8). Slope height H is related to the geometry of the mechanism through Eq. (A2). Without an insert, the stability number can be calculated from Eq. (36), after substituting b=0. For a ridge mechanism, the stability number is found considering work rates in Eqs. (33) and (35)

$$\frac{\sigma_{ci}}{\gamma H} = \frac{\sum_{j=1}^{n} \int_{\theta_{j-1}}^{\theta_{j}} \cos \theta \int_{r_{s}}^{r^{*}} \rho^{2} \left[2\sqrt{R^{2} - (\rho - r_{c})^{2}} - b^{*} \right] d\rho d\theta}{\frac{H}{\sigma_{ci}} \sum_{j=1}^{n} \left(\tau_{j} - \sigma_{nj} \tan \delta_{j} \right) \int_{\theta_{j-1}}^{\theta_{j}} \int_{r_{s}}^{r^{*}} \rho^{2} \frac{2R}{\sqrt{R^{2} - (\rho - r_{c})^{2}}} d\rho d\theta}$$
(37)

5.2. Factor of safety

Considering Eqs. (6) and (7), the demand on the components of the traction vector on the failure surface follows from the Hoek-Brown failure envelope reduced by factor of safety *F*, as illustrated in Fig. 6

$$\sigma_{nd} = \sigma_n = \sigma_{ci} \left\{ \left(\frac{1}{m_b} + \frac{\sin \delta_j}{m_b a} \right) \left[\frac{m_b a \left(1 - \sin \delta_j \right)}{2 \sin \delta_j} \right]^{\frac{1}{1 - a}} - \frac{s}{m_b} \right\}$$
(38)

and

$$\tau_d = \frac{\tau}{F} = \frac{\sigma_{ci}}{F} \left\{ \frac{\cos \delta_j}{2} \left[\frac{m_b a \left(1 - \sin \delta_j \right)}{2 \sin \delta_j} \right]^{\frac{a}{1 - a}} \right\}$$
 (39)

where rupture angle δ_j must now be expressed as a function of the demand on δ (Fig. 6)

$$\delta_i = \arctan(F \tan \delta_{di}) \tag{40}$$

In computations, angles δ_{dj} will be independent variables in an optimization process leading to evaluation of the minimum factor of safety F. The respective work rate terms take the form

$$D = \omega \sum_{j=1}^{n} \left(\tau_{dj} - \sigma_{ndj} \tan \delta_{dj} \right) \int_{\theta_{j,1}}^{\theta_{j}} \left[\int_{r_{c}}^{r} \rho^{2} \frac{2R}{\sqrt{R^{2} - (\rho - r_{c})^{2}}} d\rho + b r^{2} \right] d\theta \qquad (41)$$

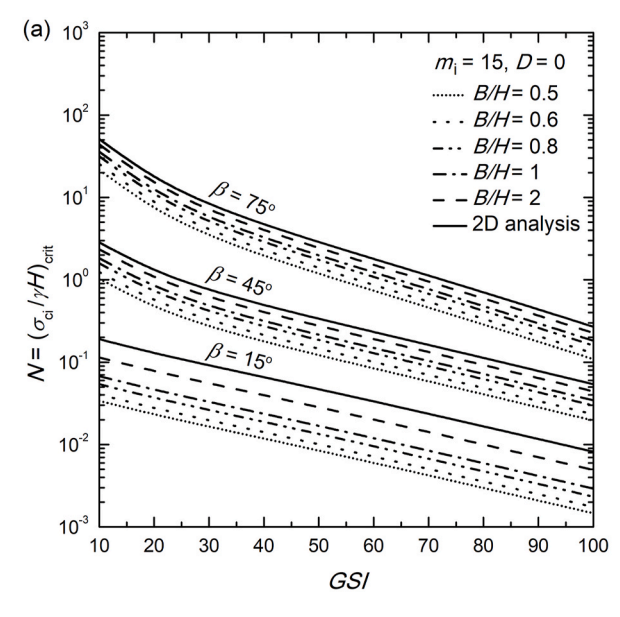
and

$$W_{\gamma} = \omega \gamma \sum_{j=1}^{n} \int_{\theta_{j-1}}^{\theta_{j}} \cos \theta \int_{r_{s}}^{r} \rho^{2} \left[2\sqrt{R^{2} - (\rho - r_{c})^{2}} + b \right] d\rho d\theta \tag{42}$$

where radius r is expressed in Eq. (10), but now needs to be calculated considering Eq. (40). Replacing the traction components in Eq. (41) with those in Eqs. (38) and (39), and substituting expressions in Eqs. (41) and (42) into Eq. (19), the following implicit equation was derived from which the factor of safety can be calculated

$$\begin{split} &\frac{\sigma_{ci}}{\gamma H} \sum_{j=1}^{n} \left\{ \frac{\cos \delta_{j}}{2F} \left[\frac{m_{b} a \left(1 - \sin \delta_{j} \right)}{2 \sin \delta_{j}} \right]^{\frac{s}{1-a}} - \left(\frac{1}{m_{b}} + \frac{\sin \delta_{j}}{m_{b} a} \right) \left[\frac{m_{b} a \left(1 - \sin \delta_{j} \right)}{2 \sin \delta_{j}} \right]^{\frac{1}{1-a}} \tan \delta_{dj} \\ &+ \frac{s}{m_{b}} \tan \delta_{dj} \right\} \int_{\theta_{j-1}}^{\theta_{j}} \left[\int_{r_{s}}^{r} \rho^{2} \frac{2R}{\sqrt{R^{2} - (\rho - r_{c})^{2}}} d\rho + b r^{2} \right] d\theta \\ &= \frac{1}{H} \sum_{j=1}^{n} \int_{\theta_{j-1}}^{\theta_{j}} \cos \theta \int_{r_{s}}^{r} \rho^{2} \left[2\sqrt{R^{2} - (\rho - r_{c})^{2}} + b \right] d\rho d\theta \end{split} \tag{43}$$

where δ_j is expressed in Eq. (40) and $\sigma_{ci}/\gamma H$ is the dimensionless group for the slope under consideration. Factors of safety for the ridge failure surface mechanism follow from Eq. (43) after making appropriate adjustments $(r \to r^*, \; \theta_0 \to \theta_0^*, \theta_n \to \theta_n^*, \; \text{and modification of } b)$, and the following implicit equation with respect to F can be used for ridge failure mechanisms



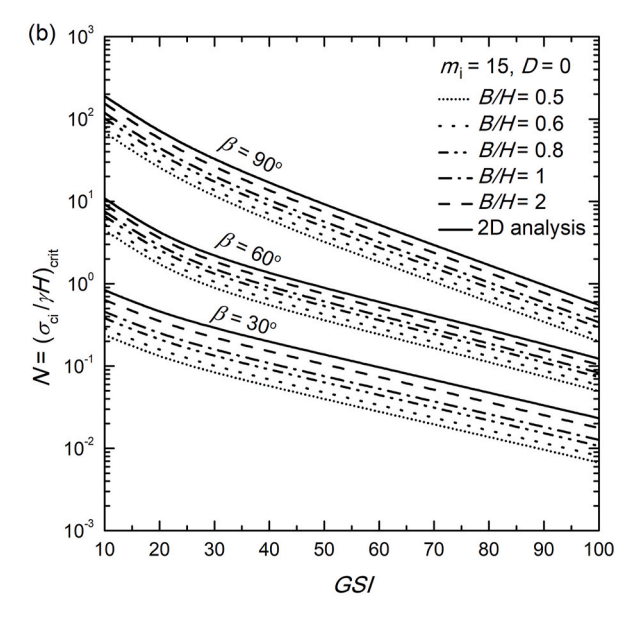


Fig. 7. Stability number for rock slopes as a function of Geological Strength Index: (a) slope inclination angles $\beta = 15^{\circ}$, 45° , and 75° , and 75° , and 90° .

$$\begin{split} &\frac{\sigma_{ci}}{\gamma H} \sum_{j=1}^{n} \left\{ \frac{\cos \delta_{j}}{2F} \left[\frac{m_{b} a \left(1 - \sin \delta_{j} \right)}{2 \sin \delta_{j}} \right]^{\frac{a}{1-a}} - \left(\frac{1}{m_{b}} + \frac{\sin \delta_{j}}{m_{b} a} \right) \left[\frac{m_{b} a \left(1 - \sin \delta_{j} \right)}{2 \sin \delta_{j}} \right]^{\frac{1}{1-a}} \tan \delta_{dj} \right. \\ &\left. + \frac{s}{m_{b}} \tan \delta_{dj} \right\} \int_{\theta_{j-1}}^{\theta_{j}} \left[\int_{r_{s}}^{r^{*}} \rho^{2} \frac{2R}{\sqrt{R^{2} - (\rho - r_{c})^{2}}} d\rho \right] d\theta \\ &= \frac{1}{H} \sum_{j=1}^{n} \int_{\theta_{j-1}}^{\theta_{j}} \cos \theta \int_{r_{s}}^{r^{*}} \rho^{2} \left[2\sqrt{R^{2} - (\rho - r_{c})^{2}} - b^{*} \right] d\rho d\theta \end{split} \tag{44}$$

6. Results and discussion

The kinematic approach of limit analysis provides rigorous bounds to the measures of slope safety: the lower bound to the stability number and the upper bound to the factor of safety. Therefore, a maximum value of $\sigma_{ci}/\gamma H$ will be sought from Eq. (36) and a minimum of the factor of safety from Eq. (43) will be searched for. In general, the optimization process for both the stability number and the factor of safety contains 2n+3 independent variables (2n+2 for toe failures): $\theta_0, \theta_a, r_0'/r_0, n$ angles δ , and n angles η , where n is the number of segments in the mechanism (angles η are illustrated in Fig. 2(a)). Number of segments n in all calculations was chosen to be 10, as further increase in n did not improve the results.

A custom-designed optimization routine was developed in a Matlab environment, in which all independent variables were varied in order to arrive at the maximum of the stability number or a minimum of the factor of safety. The first set of independent variables was generated automatically, assuring the admissibility of the mechanism. Next, the variables were subjected to a change, one by one in consecutive loops in search for a more accurate bound to the exact solution. All angle variables were modified by an initial increment of 0.1° , and ratio r'_0/r_0 by 0.01. In final calculations, these increments were reduced to 0.001° and 0.0001, respectively. The process continued until the difference between two consecutive outcomes (whether stability number or factor of safety) was less than 10^{-6} . The time of calculations is very much dependent on the initial set (guess) of independent variables. With a random first guess for a problem with 10 segments (23 variables), the computation time was typically less than 10 min for the stability number and less than 30 min for a single calculation of a factor of safety, for which governing Eq.

Table 1 Stability number $\sigma_{ci}/\gamma H$ for slopes in intact rock ($m_i = 15, D = 0$).

| β (°) | B/H | GSI | | | | |
|-------|-----|--------|--------|-------|-------|------|
| | | 20 | 40 | 60 | 80 | 100 |
| 30 | 0.5 | 0.129 | 0.057 | 0.028 | 0.014 | 0.00 |
| | 0.6 | 0.155 | 0.069 | 0.034 | 0.017 | 0.00 |
| | 0.8 | 0.206 | 0.091 | 0.044 | 0.022 | 0.01 |
| | 1 | 0.245 | 0.108 | 0.053 | 0.026 | 0.01 |
| | 2 | 0.342 | 0.150 | 0.074 | 0.036 | 0.01 |
| | 2D | 0.449 | 0.198 | 0.097 | 0.048 | 0.02 |
| 45 | 0.5 | 0.458 | 0.178 | 0.084 | 0.041 | 0.02 |
| | 0.6 | 0.549 | 0.213 | 0.101 | 0.049 | 0.02 |
| | 0.8 | 0.702 | 0.272 | 0.129 | 0.062 | 0.03 |
| | 1 | 0.813 | 0.315 | 0.149 | 0.072 | 0.03 |
| | 2 | 1.041 | 0.405 | 0.191 | 0.093 | 0.04 |
| | 2D | 1.266 | 0.493 | 0.233 | 0.113 | 0.05 |
| 60 | 0.5 | 1.627 | 0.544 | 0.243 | 0.111 | 0.05 |
| | 0.6 | 1.924 | 0.644 | 0.287 | 0.132 | 0.05 |
| | 0.8 | 2.413 | 0.810 | 0.363 | 0.165 | 0.07 |
| | 1 | 2.745 | 0.921 | 0.411 | 0.188 | 0.08 |
| | 2 | 3.382 | 1.139 | 0.509 | 0.233 | 0.10 |
| | 2D | 3.982 | 1.344 | 0.602 | 0.276 | 0.12 |
| 75 | 0.5 | 7.089 | 1.950 | 0.738 | 0.287 | 0.10 |
| | 0.6 | 8.337 | 2.292 | 0.868 | 0.337 | 0.12 |
| | 0.8 | 10.415 | 2.867 | 1.085 | 0.422 | 0.16 |
| | 1 | 11.804 | 3.253 | 1.234 | 0.480 | 0.18 |
| | 2 | 14.435 | 3.996 | 1.523 | 0.595 | 0.22 |
| | 2D | 16.873 | 4.692 | 1.796 | 0.705 | 0.27 |
| 90 | 0.5 | 24.812 | 5.944 | 1.842 | 0.602 | 0.19 |
| | 0.6 | 29.147 | 6.974 | 2.162 | 0.709 | 0.23 |
| | 0.8 | 36.809 | 8.850 | 2.733 | 0.894 | 0.29 |
| | 1 | 42.823 | 10.331 | 3.193 | 1.038 | 0.34 |
| | 2 | 55.972 | 13.527 | 4.178 | 1.356 | 0.44 |
| | 2D | 69.220 | 16.799 | 5.192 | 1.686 | 0.55 |

All results for $H/B \le 0.8$ are based on multi-cone ridge failure surface mechanism (n = 10); otherwise, multi-cone mechanism with or without insert (no ridge).

(43) is implicit (single CPU running at 1.8 GHz). These computation times were reduced about ten-fold in the successive (systematic) computations when the first guess was made based on the previous calculations with similar slope geometry and rock properties.

Stability numbers for slopes with inclination varied from 15° to 90° are presented in Fig. 7, in semi-log plots, as functions of Geological Strength Index *GSI*, all for $m_i = 15$ and disturbance index D = 0. The results are given for the failure mechanism constraint B/H from 0.5 to 2

Table 2 Comparison of stability number $\sigma_{ci}/\gamma H$ for slopes in intact rock ($m_i = 7$, D = 0, $\beta = 60^\circ$).

| B/H | Reference | GSI | GSI | | | | | | | |
|-----|-----------------------------------|--------|-------|-------|-------|-------|-------|-------|-------|--|
| | | 10 | 20 | 30 | 40 | 50 | 60 | 70 | 80 | |
| 0.8 | This study ^a | 16.428 | 5.455 | 2.749 | 1.633 | 1.029 | 0.663 | 0.432 | 0.280 | |
| | Yang and Long (2015) ^b | 14.946 | 5.060 | 2.577 | 1.541 | 0.978 | 0.629 | 0.411 | 0.268 | |
| 1 | This study ^a | 18.419 | 6.148 | 3.097 | 1.836 | 1.168 | 0.760 | 0.495 | 0.320 | |
| | Yang and Long (2015) ^b | 17.522 | 5.889 | 3.001 | 1.793 | 1.138 | 0.733 | 0.474 | 0.310 | |
| 2 | This study ^a | 22.831 | 7.617 | 3.842 | 2.290 | 1.457 | 0.947 | 0.617 | 0.399 | |
| | Yang and Long (2015) ^b | 21.293 | 7.216 | 3.676 | 2.197 | 1.395 | 0.898 | 0.592 | 0.386 | |
| 5 | This study ^a | 25.304 | 8.441 | 4.267 | 2.547 | 1.622 | 1.055 | 0.687 | 0.445 | |
| | Yang and Long (2015) ^b | 23.520 | 7.951 | 4.051 | 2.421 | 1.536 | 0.989 | 0.654 | 0.427 | |
| 10 | This study ^a | 26.089 | 8.706 | 4.404 | 2.630 | 1.674 | 1.089 | 0.710 | 0.460 | |
| | Yang and Long (2015) ^b | 24.251 | 8.180 | 4.169 | 2.492 | 1.581 | 1.019 | 0.674 | 0.440 | |

^a Calculations with Hoek-Brown strength criterion and multi-cone mechanism (n = 10); ridge mechanism for B/H = 0.8, otherwise multi-cone mechanism with or without insert (no ridge).

Table 3 Comparison of stability number $\sigma_{ci}/\gamma H$ for slopes in intact rock ($m_i = 15$, D = 0, $\beta = 60^\circ$).

| B/H | Reference | GSI | | | | | | | | | | |
|-----|-----------------------------------|--------|-------|-------|-------|-------|-------|-------|-------|--|--|--|
| | | 10 | 20 | 30 | 40 | 50 | 60 | 70 | 80 | | | |
| 0.8 | This study ^a | 6.567 | 2.413 | 1.290 | 0.810 | 0.537 | 0.363 | 0.246 | 0.165 | | | |
| | Yang and Long (2015) ^b | 6.085 | 2.213 | 1.194 | 0.753 | 0.501 | 0.340 | 0.231 | 0.156 | | | |
| 1 | This study ^a | 7.530 | 2.745 | 1.477 | 0.921 | 0.609 | 0.411 | 0.279 | 0.188 | | | |
| | Yang and Long (2015) ^b | 7.184 | 2.613 | 1.392 | 0.877 | 0.583 | 0.396 | 0.269 | 0.182 | | | |
| 2 | This study ^a | 9.230 | 3.382 | 1.824 | 1.139 | 0.754 | 0.509 | 0.345 | 0.233 | | | |
| | Yang and Long (2015) ^b | 8.669 | 3.155 | 1.703 | 1.073 | 0.714 | 0.484 | 0.330 | 0.223 | | | |
| 5 | This study ^a | 10.228 | 3.753 | 2.026 | 1.266 | 0.838 | 0.566 | 0.384 | 0.260 | | | |
| | Yang and Long (2015) ^b | 9.637 | 3.507 | 1.876 | 1.183 | 0.787 | 0.534 | 0.363 | 0.246 | | | |
| 10 | This study ^a | 10.548 | 3.872 | 2.091 | 1.307 | 0.865 | 0.584 | 0.397 | 0.268 | | | |
| | Yang and Long (2015) ^b | 9.941 | 3.616 | 1.930 | 1.217 | 0.809 | 0.549 | 0.374 | 0.253 | | | |

^a Calculations with Hoek-Brown strength criterion and multi-cone mechanism (n = 10); ridge mechanism for B/H = 0.8, otherwise multi-cone mechanism with or without insert (no ridge).

and for a 2D analysis. Not surprisingly, the stability number is strongly influenced by GSI and the slope inclination. The strong dependence on GSI is consistent with stability analyses of tunnel roofs in intact rock. 26,27 For comparative purposes, numerical values are given in Table 1. The difference in the stability number from a 3D analysis with B/H=0.5 and the 2D analysis is roughly three-fold: a significant underestimation of rock slope stability if 2D analyses are used for narrow slopes.

The authors are not aware of any other results from 3D analyses of

rock slopes that would be obtained without some approximation of the Hoek-Brown envelope. The results obtained here are compared to those by Yang and Long, ⁸ who presented their results for a wide range of parameters albeit with linear approximation of the H–B envelope. The comparisons are presented in Tables 2 and 3 for 60° slopes in rocks with *GSI* varied from 10 to 80 and index m_i of 7 and 15. In all cases, the method of calculations offered in this paper yields a higher stability number N, thus more accurate, since the kinematic analysis provides a lower bound to N. The difference in the tables does not exceed 10%, but

Table 4 Comparison of stability number $\sigma_{ci}/\gamma H$ for vertical narrow slopes, calculated for three failure mechanisms ($m_i = 15$, D = 0, $\beta = 90^\circ$).

| B/H | Face failure | GSI | | | | | | | | | |
|-----|-------------------------|---------|--------|--------|-------|-------|-------|-------|-------|-------|-------|
| | | 10 | 20 | 30 | 40 | 50 | 60 | 70 | 80 | 90 | 100 |
| 0.3 | Ridge ^a | 42.735 | 15.434 | 7.148 | 3.719 | 2.046 | 1.151 | 0.654 | 0.375 | 0.214 | 0.123 |
| | Multi-cone ^b | 36.834 | 13.158 | 6.051 | 3.180 | 1.760 | 0.997 | 0.570 | 0.328 | 0.188 | 0.108 |
| | Linear ^c | 36.475 | 13.058 | 6.003 | 3.144 | 1.747 | 0.990 | 0.564 | 0.323 | 0.186 | 0.107 |
| 0.4 | Ridge ^a | 56.033 | 20.234 | 9.372 | 4.849 | 2.611 | 1.503 | 0.857 | 0.491 | 0.281 | 0.162 |
| | Multi-cone ^b | 49.112 | 17.543 | 8.068 | 4.240 | 2.347 | 1.329 | 0.761 | 0.437 | 0.251 | 0.145 |
| | Linear ^c | 48.616 | 17.404 | 8.003 | 4.205 | 2.330 | 1.320 | 0.752 | 0.431 | 0.248 | 0.142 |
| 0.5 | Ridge ^a | 68.728 | 24.812 | 11.498 | 5.944 | 3.188 | 1.842 | 1.050 | 0.602 | 0.344 | 0.199 |
| | Multi-cone ^b | 61.390 | 21.929 | 10.085 | 5.300 | 2.934 | 1.663 | 0.951 | 0.546 | 0.314 | 0.181 |
| | Linear ^c | 60.995 | 21.724 | 10.021 | 5.262 | 2.914 | 1.649 | 0.940 | 0.539 | 0.309 | 0.178 |
| 0.6 | Ridge ^a | 80.718 | 29.147 | 13.508 | 6.974 | 3.863 | 2.162 | 1.233 | 0.709 | 0.405 | 0.233 |
| | Multi-cone ^b | 73.644 | 26.329 | 12.132 | 6.365 | 3.543 | 1.993 | 1.141 | 0.655 | 0.376 | 0.217 |
| | Linear ^c | 72.945 | 26.126 | 12.034 | 6.326 | 3.512 | 1.979 | 1.128 | 0.646 | 0.371 | 0.214 |
| 0.8 | Ridge ^a | 101.922 | 36.809 | 17.056 | 8.850 | 4.877 | 2.733 | 1.561 | 0.894 | 0.511 | 0.294 |
| | Multi-cone ^b | 99.098 | 35.609 | 16.476 | 8.587 | 4.733 | 2.668 | 1.522 | 0.874 | 0.502 | 0.289 |
| | Linear ^c | 98.191 | 35.308 | 16.339 | 8.518 | 4.683 | 2.639 | 1.504 | 0.860 | 0.493 | 0.283 |

^a Multi-cone ridge failure surface mechanism (n = 10).

b Linear approximation of Hoek-Brown criterion; to make the comparison, a reciprocal of results in Yang and Long (2015) was taken, multiplied by s^{-0.5}.

b Linear approximation of Hoek-Brown criterion; to make the comparison, a reciprocal of results in Yang and Long (2015) was taken, multiplied by s^{-0.5}.

 $^{^{\}rm b}$ Multi-cone failure surface mechanism (n=10, no ridge).

^c Calculated with linear approximation of the Hoek-Brown strength criterion.

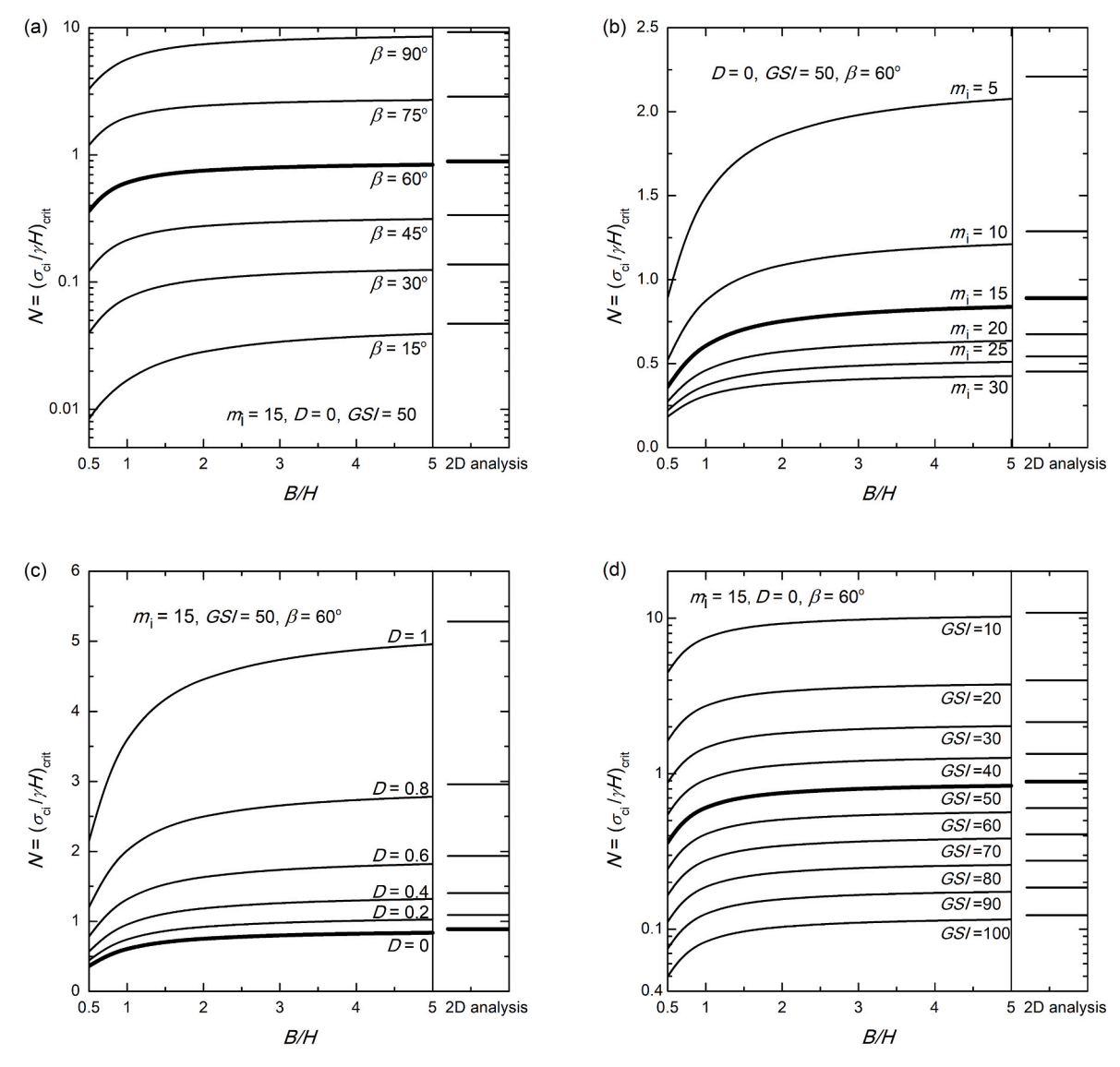


Fig. 8. Stability number for rock slopes as a function of mechanism width constrain B/H: (a) the influence of slope inclination angle β , (b) rock type m_i , (c) disturbance factor D, and (d) Geological Strength Index (GSI).

the largest difference occurs for very stringent constraints on the mechanism width (B/H < 0.8), for which no solutions were shown by Yang and Long.⁸

The study indicated that for very narrow slopes the improvement in N obtained using the proposed ridge failure surface mechanism can be greater than 10%. Very narrow vertical slopes, with constraint B/H in the range from 0.3 to 0.8, were analyzed using the ridge failure surface mechanism in Fig. 5, multi-cone face failure mechanism in Fig. 4, and the mechanism with a linearized Hoek-Brown strength envelope. In the former two cases, the parametric form of the Hoek-Brown failure criterion was used, and both analyses were carried out without compromising the rock's nonlinear dependency of the shear strength on pressure. The outcome of this study is presented in Table 4. By using the ridge failure mechanism illustrated in Fig. 5, the improvement in stability number N can exceed 15%, compared to a more traditional face failure mechanism in Fig. 4. The difference in the stability number from analyses based on the multi-cone face failure mechanism and that based on linearization of the Hoek-Brown strength envelope is very small for vertical slopes (Table 4), but it is larger for gentler slopes.

The effects of the slope inclination angle and the Hoek-Brown model parameters on the stability number for rock slopes are illustrated in Fig. 8. Of course, the stability number increases with an increase in slope

inclination. The influence of the rock properties is as expected: the weaker the rock type (m_i) , and the lower the Geological Strength Index (GSI), the higher the stability number. The majority of calculations in the paper were carried out for slopes in an intact, minimally disturbed rock (D=0), with the exception of the results in Fig. 8(c). In rock excavations by blasting, the disturbance is not uniform through all of the rock, and it would be inappropriate to assume uniform disturbance factor D throughout the rock, as pointed out by Hoek and Brown.² The chart in Fig. 8(c), with each curve found for one value of D, is presented solely for the purpose of indicating that the tendency of the numerical outcome is consistent with expectations (increase in the stability number with an increase in disturbance factor *D*). One should expect, however, that the results in this chart, particularly for larger factors D, are over-conservative. Assessing the quantitative influence of the disturbance factor requires an analysis with non-uniform distribution of factor D, but this was beyond the scope of this study.

The influence of the rock properties is as expected: the more disturbed the rock (D), the weaker the rock type (m_i) , and the lower the Geological Strength Index (GSI), the higher the stability number.

The factor of safety is a more intuitive measure of stability than the stability number, and it is presented in Fig. 9 as a function of dimensionless group $\sigma_{\rm ci}/\gamma H$. The safety factors for slope width constraint B/H

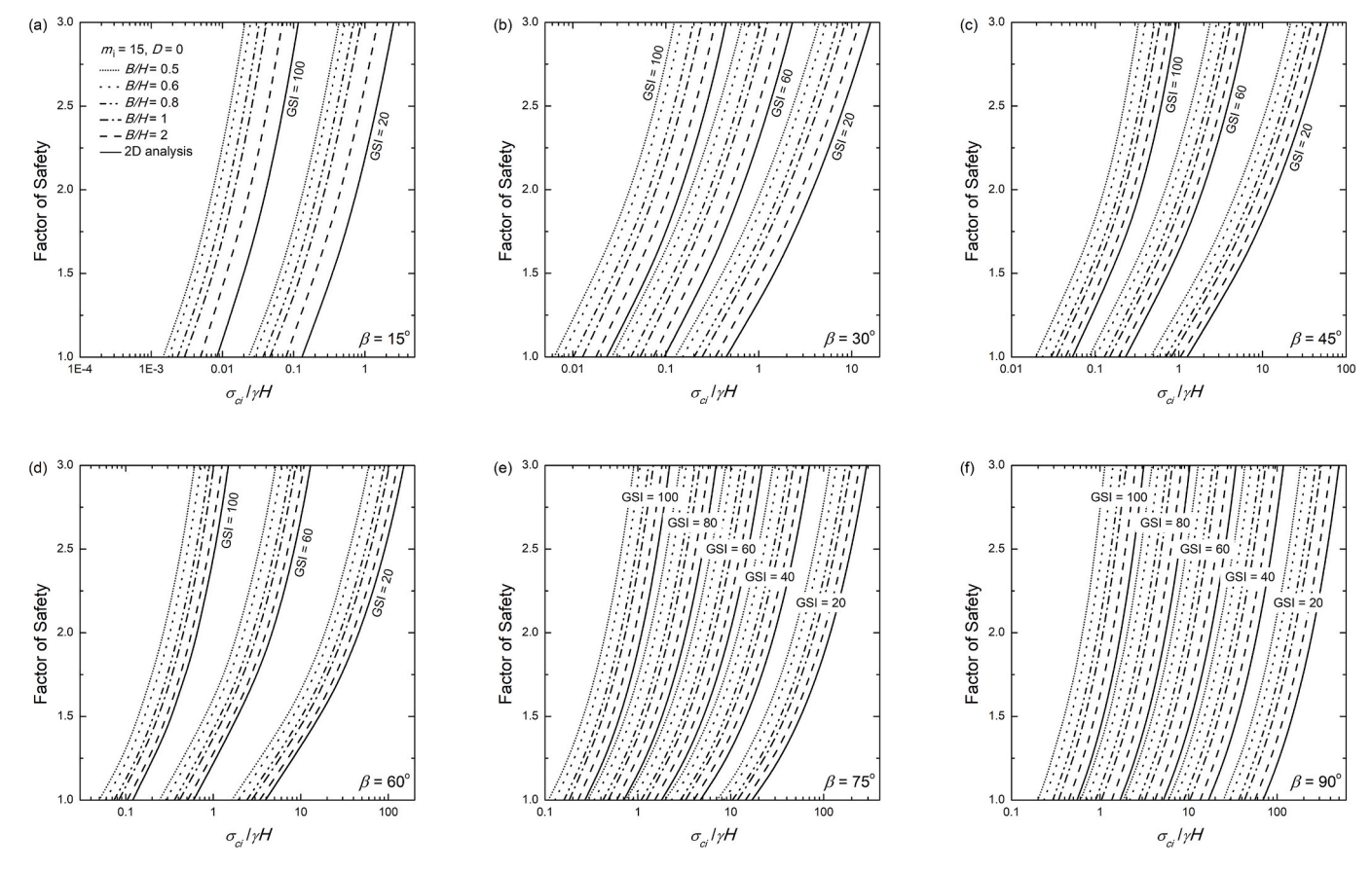


Fig. 9. Factor of safety for rock slopes with inclination angles in the range from $\beta=15^{\circ}$ through $\beta=90^{\circ}$.

Table 5 Factors of safety for slopes in intact rock with $\sigma_{ci}/\gamma H = 10$ ($m_i = 15$, D = 0).

| GSI | β (°) | B/H | | | | | | | | |
|-----|-------|--------|--------|--------|--------|--------|-------|--|--|--|
| | | 0.5 | 0.6 | 0.8 | 1 | 2 | 2D | | | |
| 20 | 15 | 10.970 | 7.082 | 6.555 | 6.184 | 5.293 | 4.576 | | | |
| | 30 | 3.734 | 3.547 | 3.285 | 3.126 | 2.848 | 2.649 | | | |
| | 45 | 2.410 | 2.289 | 2.135 | 2.048 | 1.915 | 1.816 | | | |
| 40 | 30 | 5.376 | 5.047 | 4.613 | 4.378 | 3.949 | 3.654 | | | |
| | 45 | 3.523 | 3.313 | 3.052 | 2.914 | 2.695 | 2.542 | | | |
| | 60 | 2.545 | 2.390 | 2.193 | 2.097 | 1.947 | 1.845 | | | |
| 60 | 45 | 5.497 | 5.052 | 4.516 | 4.241 | 3.820 | 3.534 | | | |
| | 60 | 4.087 | 3.762 | 3.373 | 3.179 | 2.883 | 2.675 | | | |
| | 75 | 3.202 | 2.937 | 2.618 | 2.455 | 2.201 | 2.024 | | | |
| 80 | 60 | 8.026 | 7.260 | 6.385 | 5.929 | 5.182 | 4.642 | | | |
| | 75 | 6.663 | 6.010 | 5.258 | 4.862 | 4.215 | 3.741 | | | |
| | 90 | 5.710 | 5.113 | 4.401 | 4.018 | 3.391 | 2.932 | | | |
| 100 | 75 | 17.499 | 15.760 | 13.713 | 12.577 | 10.566 | 8.966 | | | |
| | 90 | 15.472 | 13.817 | 11.854 | 10.770 | 8.864 | 7.354 | | | |

All results for $B/H \le 0.8$ based on multi-cone ridge failure surface mechanism (n=10); otherwise, multi-cone mechanism with or without insert (no ridge).

up to 0.8 are all based on the multi-cone ridge failure surface mechanism (Fig. 5); all remaining factors of safety are from the analysis with the multi-cone mechanism (Fig. 2 or Fig. 3). Charts (a) through (f) show factors of safety for slopes of inclination angle β ranging from 15° to 90° . When F=1, the value of the dimensionless group $\sigma_{\rm ci}/\gamma H$ becomes equal to the stability number. The results are shown for rock disturbance factor $D=0, m_{\rm i}=15,$ and slope width constraint B/H from 0.5 to 2.0, and for a 2D analysis. To preserve clarity in the charts, results are presented only for selected values of GSI. Numerical values of the factors of safety are presented in Tables 5 and 6.

Table 6 Factors of safety for slopes in intact rock with $\sigma_{ci}/\gamma H = 1$ ($m_i = 15$, D = 0).

| GSI | β (°) | B/H | | | | | | | | |
|-----|-------|-------|-------|-------|-------|-------|-------|--|--|--|
| | | 0.5 | 0.6 | 0.8 | 1 | 2 | 2D | | | |
| 20 | 15 | 3.911 | 3.681 | 3.369 | 3.122 | 2.618 | 2.185 | | | |
| | 30 | 1.954 | 1.844 | 1.692 | 1.608 | 1.444 | 1.317 | | | |
| | 45 | 1.267 | 1.201 | 1.115 | 1.066 | 0.988 | 0.929 | | | |
| 40 | 30 | 2.656 | 2.505 | 2.298 | 2.184 | 1.961 | 1.789 | | | |
| | 45 | 1.738 | 1.644 | 1.521 | 1.450 | 1.342 | 1.264 | | | |
| | 60 | 1.200 | 1.142 | 1.067 | 1.025 | 0.961 | 0.914 | | | |
| 60 | 45 | 2.245 | 2.117 | 1.956 | 1.863 | 1.722 | 1.617 | | | |
| | 60 | 1.577 | 1.491 | 1.384 | 1.328 | 1.239 | 1.176 | | | |
| | 75 | 1.118 | 1.052 | 0.972 | 0.928 | 0.862 | 0.815 | | | |
| 80 | 60 | 2.292 | 2.131 | 1.930 | 1.830 | 1.679 | 1.574 | | | |
| | 75 | 1.730 | 1.604 | 1.445 | 1.364 | 1.240 | 1.152 | | | |
| | 90 | 1.321 | 1.209 | 1.063 | 0.980 | 0.848 | 0.754 | | | |
| 100 | 75 | 3.185 | 2.893 | 2.551 | 2.373 | 2.093 | 1.892 | | | |
| | 90 | 2.737 | 2.393 | 2.074 | 1.900 | 1.622 | 1.421 | | | |

All results for $B/H \le 0.8$ based on multi-cone ridge failure surface mechanism (n = 10); otherwise, multi-cone mechanism with or without insert (no ridge).

7. Conclusions

Stability of rock slopes has been a popular topic of research in rock engineering, yet the authors were not able to identify three-dimensional analyses in the literature that would focus on the quantitative measures of slope stability in intact rock, while being faithful to the nonlinear pressure dependency of the rock shear strength. The most commonly used failure criterion for rocks is that introduced by Hoek and Brown¹⁷ in 1980; the latest version of this criterion^{1,2} was used in this paper. This limit state criterion is a function of the major and minor principal effective stresses. Stability analyses involving geomaterials often call for the strength criterion expressed as the Mohr hypothesis with the shear

strength as an explicit function of the normal effective stress $\tau = f(\sigma_n')$. The Hoek-Brown criterion cannot be easily transformed into the Mohr-type hypothesis, but the authors used its parametric form to preserve its nonlinearity in the analysis, whereas in the majority of other approaches the nonlinear criterion was substituted by a linear approximation before the analysis was carried through.

Computational stability numbers obtained in this study using the new approach are more accurate than those available in the literature. This assessment is possible, because the method used in the paper yields a rigorous lower bound to the true stability numbers, while the numbers calculated are larger than those found in available literature. The new approach also made it possible to arrive at upper bound factors of safety for rock slopes, which previously was done in 3D analyses only after the nonlinear strength envelope was substituted with a linear approximation.

A new mechanism of failure was found for slopes subjected to a stringent restriction on its width ($B/H \le 0.8$). For very wide slopes, a mechanism with a 2D insert was developed earlier, ³ whereas for very narrow slopes, a mechanism was now constructed by removing a slice

from the central portion of the multi-cone rotating block. The failure surface formed by the two remaining halves joined together has a distinct ridge at the symmetry plane, and it was referred to as the ridge failure surface. This mechanism was found to be quite efficient, yielding stability numbers increased by as much as 17% compared to the commonly used face failure mechanism for narrow slopes.

Declaration of competing interest

The authors declare that they have no known competing financial interests or personal relationships that could have appeared to influence the work reported in this paper.

Acknowledgements

The work presented in this paper was carried out while the authors were supported by the National Science Foundation, Grant No. CMMI-1901582 and the Horace Rackham School of Graduate Studies at the University of Michigan. This support is greatly appreciated.

Appendix

Angle θ_c was calculated from geometric relationships in Fig. 2, and it can be expressed as

$$\theta_c = \arctan \frac{r_n \sin \theta_n - H}{r_n \cos \theta_n + H \cot \beta} \tag{A1}$$

The height of slope H is uniquely related to radius r_0 as

$$H = r_0 e^{\frac{\sum_{j=1}^{n} (\theta_j - \theta_{j-1}) tan\delta_j}{sin\theta_n - r_0 sin\theta_0}}$$
(A2)

where angle $\theta_j - \theta_{j-1}$ is equal to η_j , as marked in Fig. 2(a). Radial coordinate r_s of the slope contour is determined in three distinct regions: B₀C, CA (Fig. 2) and AB_n (for below-toe failures, Fig. 3)

$$r_{s}(\theta) = \begin{cases} r_{0} \frac{\sin\theta_{0}}{\sin\theta} &, \quad B_{0}C: \theta_{0} < \theta \leq \theta_{c} \\ r_{n} \frac{\sin\theta_{a} + \cos\theta_{a} \tan \beta}{\sin \theta + \tan \beta \cos \theta} &, \quad CA: \theta_{c} < \theta \leq \theta_{a} \\ r_{a} \frac{\sin\theta_{a}}{\sin \theta} &, \quad AB_{n}: \theta_{a} < \theta \leq \theta_{n} \text{ (below - toe only)} \end{cases}$$
(A3)

with angles θ_c (Eq. (A1)) and θ_a (independent variable) illustrated in Figs. 2 and 3, and r_a is found in Eq. (17).

References

- Hoek E, Carranza-Torres C, Corkum B. Hoek-Brown failure criterion-2002 edition. Proceedings of NARMS-Tac. 2002;1:267–273.
- 2 Hoek E, Brown E. The Hoek–Brown failure criterion and GSI–2018 edition. Journal of Rock Mechanics and Geotechnical Engineering. 2019;11(3):445–463.
- 3 Michalowski RL, Drescher A. Three-dimensional stability of slopes and excavations. Geotechnique. 2009;59(10):839–850.
- 4 Drescher A, Christopoulos C. Limit analysis slope stability with nonlinear yield condition. Int J Numer Anal Methods GeoMech. 1988;12(3):341–345.
- 5 Collins IF, Gunn CIM, Pender MJ, Yan W. Slope stability analyses for materials with a non-linear failure envelope. Int J Numer Anal Methods GeoMech. 1988:12(5):533–550.
- non-linear failure envelope. *Int J Numer Anal Methods GeoMech.* 1988;12(5):533–550. 6 Zhang X, Chen W. Stability analysis of slopes with general nonlinear failure criterion.
- 7 Xu J, Yang X. Seismic stability analysis and charts of a 3D rock slope in Hoek–Brown media. Int J Rock Mech Min Sci. 2018;112:64–76.

Int J Numer Anal Methods GeoMech. 1987;11(1):33-50.

- 8 Yang X-L, Long Z-X. Seismic and static 3D stability of two-stage rock slope based on Hoek–Brown failure criterion. *Can Geotech J.* 2015;53(3):551–558.
- 9 Yang X-L. Effect of pore-water pressure on 3D stability of rock slope. Int J GeoMech. 2017;17(9), 06017015.
- 10 Xu J, Pan Q, Yang X, Li W. Stability charts for rock slopes subjected to water drawdown based on the modified nonlinear Hoek-Brown failure criterion. *Int J GeoMech.* 2018;18(1), 04017133.

- 11 Pan Q, Jiang Y-J, Dias D. Probabilistic stability analysis of a three-dimensional rock slope characterized by the Hoek-Brown failure criterion. *J Comput Civ Eng.* 2017;31 (5), 04017046.
- 12 Michalowski RL, Park D. Stability assessment of slopes in rock governed by the Hoek-Brown strength criterion. Int J Rock Mech Min Sci. 2020;127:104217.
- 13 Chen W-F. Limit Analysis and Soil Plasticity. New York: Elsevier; 1975.
- 14 Chen WF, Drucker DC. Bearing capacity of concrete blocks or rock. J Eng Mech Div. 1969;95(4):955–978.
- 15 Michalowski RL. Limit analysis of quasi-static pyramidal indentation of rock. Int J Rock Mech Min Sci. 1985;22(1):31–38.
- 16 Fraldi M, Guarracino F. Limit analysis of collapse mechanisms in cavities and tunnels according to the Hoek–Brown failure criterion. *Int J Rock Mech Min Sci.* 2009;46(4): 665–673.
- 17 Hoek E, Brown ET. Empirical strength criterion for rock masses. J Geotech Eng Div. 1980;106(9):1013–1035.
- 18 Balmer G. A general analysis solution for Mohr's envelope. Proc ASTM. 1952;52: 1260–1271.
- 19 Kumar P. Shear failure envelope of Hoek-Brown criterion for rockmass. Tunn Undergr Space Technol. 1998;13(4):453–458.
- 20 Taylor D. Stability of Earth Slopes. vol. 24. J Boston Society of Civil Engineers; Reprinted in: Contributions to Soil Mechanics, 1925 to 1940 (337-386); 1937: 197–246.
- 21 Li A, Merifield R, Lyamin A. Stability charts for rock slopes based on the Hoek–Brown failure criterion. Int J Rock Mech Min Sci. 2008;45(5):689–700.
- 22 Michalowski RL. Upper-bound load estimates on square and rectangular footings. Geotechnique. 2001;51(9):787–798.

- 23 Michalowski RL. Stability of intact slopes with tensile strength cut-off. Geotechnique. 2017;67(8):720-727.
- 24 Park D, Michalowski RL. Three-dimensional stability analysis of slopes in hard soil/ soft rock with tensile strength cut-off. Eng Geol. 2017;229:73-84.
- 25 Park D, Michalowski RL. Intricacies in three-dimensional limit analysis of earth slopes. Int J Numer Anal Methods GeoMech. 2018;42(17):2109-2129.
- 26 Park D, Michalowski RL. Roof stability in deep rock tunnels. Int J Rock Mech Min Sci. 2019;124:1–12, 104139.

 27 Park D, Michalowski RL. Three-dimensional roof collapse analysis in circular tunnels
- in rock. Int J Rock Mech Min Sci. 2020;128:104275.